24th EUROPEAN ROTORCRAFT FORUM
Marseilles, France - 15th-17th September 1998

Paper No. DY-15

Recent Rotor Dynamics Predictions at Sikorsky Aircraft

James M. Wang
Senior Dynamicist

Sikorsky Aircraft Corporation
United Technologies Corporation
Stratford, CT

Analytical predictions for different Sikorsky Aircraft rotor designs are presented. Their accuracy has been validated by comparing to flight test, whirl test, and wind tunnel test data. The correlation include blade frequencies, rotor stability, air and ground resonance, blade displacement, pushrod loads, blade bending loads, vibratory hub loads and active control. Results are shown for the Sikorsky Black Hawk with an articulated main rotor, Comanche with a bearingless main rotor, experimental S-76 bearingless main rotor, Sikorsky variable diameter tiltrotor, and BO-105 with IBC.

Introduction

One of the future challenges in the rotorcraft industry is to improve the analytical methodology, such that the characteristics of a new helicopter design can be predicted accurately before it is built. By doing so, expensive wind tunnel test, whirl test, and flight test hours can be minimized. Of all the simulation disciplines, the rotor dynamics is considered as one of the most difficult areas to predict accurately. The aerodynamic environment of a rotor involves transonic flow, subsonic flow, rotational flow, unsteady flow, dynamic stall and blade-vortex interaction all existing simultaneously. It has been said that a helicopter rotor encompasses every kind of fluid dynamic phenomenon, with the exception of hypersonic flow. The rotor structure is also a challenge to model accurately. Modern rotor blades are highly twisted, made of composite material, and feature swept tips for performance improvement and tuning weight for vibration reduction. The strong centrifugal force and Coriolis force complicate the modeling by coupling flap, lag and torsion motions. The control system and rotating pushrod provide additional challenges by introducing a flexible, redundant load path.

The ability to predict rotor characteristics accurately is the critical chain for flight simulations, handling qualities analyses, flight control law designs, vibration control studies, acoustic calculations, helicopter stability predictions, performance estimations, and structural designs. Many comprehensive codes have been written in the last two decades for predicting rotor dynamics. References 1-6 provide insightful descriptions of six modern comprehensive codes. The results in [1-6] show the predictive capabilities have improved in the last decade. However, Ref. 7 illustrates some of the challenges that still exist.

At Sikorsky Aircraft, great strides have been made toward obtaining more accurate rotor dynamics predictions. Currently, three in-house aeroelastic analyses (RDYNE, KTRAN, and UMARC/S) are used [7]. Sikorsky is also working with the US army in developing and validating the 2GCHAS [1]. Having four analyses offers a distinct advantage for cross-checking each other's answer. Since all four analyses are based on different methodologies, they permit the same rotor to be examined via different approaches. All four analyses are constantly validated against test data in order to improve their precision.

For example, prior to the maiden flight of the Comanche helicopter, Sikorsky has conducted a joint wind tunnel test [8] with NASA to obtain a comprehensive data set that can also be used for code validation. A one-of-a-kind experimental bearingless main rotor (BMR) base on the diameter and blades for an Sikorsky S-76 was used [8]. With the help of extensive correlation [9-13] against the S-76 BMR, many theoretical enhancements have been added to the codes by Sikorsky during the last five years. This results in improved BMR predictions for all three in-house analyses. The reward was Sikorsky could predict the dynamics of the Comanche aircraft before its maiden flight. The successful correlation for the Comanche is shown in Ref. 14.

Description of Sikorsky Analyses

Three separate analyses have been refined at Sikorsky to predict rotor dynamics. The three aeroelastic codes use different solution techniques, and each has its strengths and weaknesses. A brief description of the three computer programs is given here.

KTRAN

KTRAN was developed at Sikorsky Aircraft for the prediction of blade frequencies, blade loads, pushrod loads and vibratory hub loads. The analysis includes coupled elastic flap, lag and torsion degrees of freedom. Fuselage dynamics and hub motions are not included. The blade equations of motion are solved using the finite segment transfer matrix method. For example, Fig. 1 illustrates how a bearingless rotor is modeled as a multiple load path system with many discrete beam elements for the blade and flexbeam, and many beam elements for the torque tube.

Control system stiffness is modeled with a torsional spring connecting the torque tube to the ground. The snubber/damper is modeled as a linear spring and damper system linked between the torque tube and the flexbeam. The spring/damper model rotates with the torque tube.

Blade element theory and airfoil table lookup are used for aerodynamic calculations. Rotor induced inflow is accounted for by the geometric influence coefficients derived from the UTRC FREEWAKE program [15]. The wake modeling enhances the prediction of higher harmonic aerodynamic forces. A harmonic balance method is used to solve the periodic-coefficient equations. The analysis can be trimmed to converge on prescribed rotor thrust and rotor moments, or to prescribed control settings.

Unlike most finite element analyses, the transfer matrix method requires a compatibility of the displacement and slope, as well as the forces and moments between elements. One advantage of the transfer matrix method is that the shear forces and bending moments are known immediately when the response is solved. A second advantage of the transfer matrix method is its speed. The matrix size for the blade equation is always the same as the number of state variables used for each element; it is independent of the number of elements used. As shown in Fig. 2, there are 10 states at each end of the element. The displacements and slopes are x = [v, v', w, w', f], and the forces and moments are F = [Fy, Mz, Fz, My, Mx]. For example, the displacements and forces at the left and right ends of element number one are related by a 10x10 transfer matrix T_{21}.

$$\begin{Bmatrix} x \\ F \end{Bmatrix}_2 = [T_{21}] \begin{Bmatrix} x \\ F \end{Bmatrix}_1$$

If n elements are used, then the blade equation simply becomes:

$$\begin{Bmatrix} x \\ F \end{Bmatrix}_n = [T_{(n,n-1)}] \cdots [T_{21}] \begin{Bmatrix} x \\ F \end{Bmatrix}_1$$

$$= [T_{n1}] \begin{Bmatrix} x \\ F \end{Bmatrix}_1$$

The disadvantage of the transfer matrix method is that if a new load path is added to the rotor design, the above equation must be rewritten to satisfy the compatibility at the junction.

UMARC/S

The Sikorsky version of the University of Maryland Advanced Rotorcraft Code (UMARC/S) is used extensively for predicting frequencies, blade loads, vibratory hub loads, and stability. UMARC [5] is based on a finite element method in space and time. Shaft motions are not included in the response calculations. The blade is assumed to be an elastic beam undergoing flatwise bending, chordwise bending, elastic twist and axial extension. This Bernoulli-Euler beam is allowed small strains and

moderate deflections. Due to the moderate deflection assumption, the equations contain nonlinear structural, inertial and aerodynamic terms. Each element has fifteen degrees of freedom. Between elements there is a continuity of displacement and slope.

For example, Fig. 2 illustrates how UMARC/S is used to model the Sikorsky Variable Diameter Tiltrotor (VDTR). The VDTR is a very unique design: its blades are fully extended during hover to maximize hover efficiency. During airplane mode, the blades are retracted to 67% of the maximum diameter to improve cruise efficiency.

In UMARC, the BMR snubber/damper is modeled in the same fashion as in KTRAN. The aerodynamic modeling used includes the Drees linear inflow, a quasi-steady strip theory, the Leishman and Beddoes 2-D unsteady aerodynamic model for capturing the unsteady shed wake, trailing edge separation and dynamic stall, and a Scully [5] or Egolf [15] free wake to capture the 3-D trailed wake and higher harmonic forcing function. Experimentally measured blade airload and flow field calculated from other analyses can also be used.

Two methods have been added to Sikorsky UMARC/S to calculate the bending moments [10]. The modal method uses the flatwise, chordwise, and torsional stiffness (EI_y, EI_z, and GJ) and the derivatives (w", v", and ϕ') calculated at the finite element Gaussian integration points to get the bending moments. Once the response has been calculated, the curvatures w", v", and ϕ' are known everywhere on the blade, flexbeam and torque tube. This method is independent of rotor type (articulated, hingeless or bearingless).

The force summation method sums up the aerodynamic and inertial loads from the spanwise elements. To find the moments inside the BMR flexbeam or the torque tube, the loads from the "redundant" path must be subtracted [10].

For stability analysis, the nonlinear blade equations are linearized about the equilibrium blade response to obtain the perturbation equations for each blade. These perturbation equations, along with the Pitt and Peters dynamic inflow equations and coupled blade/fuselage equations (if fuselage motions are included) are transformed to the fixed reference frame using a multiblade coordinate transformation. In hover, the stability roots of the constant coefficient matrix are obtained via conventional eigen analysis. For forward flight, Floquet theory is used to obtain the stability of the periodic system. This code can also calculate the stability of a rotor with dissimilar blades [16, 17].

RDYNE

The Rotorcraft Dynamics Analysis (RDYNE) [6] is a comprehensive rotor trim/time history program developed at Sikorsky. It uses a modal analysis method. The blade modes can be calculated internally, or imported from another analysis. The blade response solution is obtained by a time-marching procedure. The aerodynamic modeling includes the Leishman and Beddoes unsteady aerodynamics and the Egolf FREEWAKE [15]. Experimentally measured airload can be used in lieu of the internally calculated airload. The blade loads and hub loads can be calculated using either the modal method or the force summation method.

The integrated time responses are post-processed via a FFT/Moving Block software to obtain the modal frequencies and stability. The mass, damping and stiffness matrices from the converged solution can also be extracted to permit a stability analysis using the Floquet theory for forward flight or eigen analysis for hover.

RDYNE and KTRAN include a full nonlinear model for the hydraulic lag damper. This permits calculation of the damper loads and pushrod loads without any damping estimation from the user. RDYNE also permits hub motions during the blade response calculation. RDYNE is used extensively at Sikorsky for load and stability predictions [11, 18, 19].

All three analyses can be run quickly on the IBM RISC workstation. Since all three analyses utilize different input formats, a translator program has been written to automatically convert the input from one code to another code.

Results and Discussion

Frequency and Stability Predictions

Figure 3 shows the frequency correlation for the Sikorsky Variable Diameter Tiltrotor model [20]. Even with such a unique structural design, the analysis predicts frequencies well under all operating

conditions. The stability and load prediction for the VDTR are shown in Ref. 20. Figure 4 shows the frequency correlation for the Sikorsky S-76 BMR. Both KTRAN and UMARC/S show good results. The data were obtained via three different techniques: swashplate cyclic excitation, harmonic crossing, and chirp excitation [14].

Figure 5 shows the coupled rotor-fuselage air resonance prediction for the Boeing/Sikorsky Comanche model. The analysis compares favorably against wind tunnel data. Figure 6 shows the isolated rotor stability correlation for the Sikorsky full-scale S-76 BMR in hover and in forward flight at the NASA Ames 40'x80' wind tunnel.

Rotor Response Prediction

Figures 7 and 8 show the predicted and measured on-axis (Mx/θ_{1C}) and off-axis (My/θ_{1C}) rotor response to a prescribed cyclic command for the S-76 BMR. Mx is the hub rolling moment and My is the hub pitching moment. θ_{1C} is the lateral cyclic input. UMARC/S was used to generates a time history simulation of 200 rotor revolutions. The predicted time histories were then processed using CIFER [13]. The rotor was excited in the analysis and in the wind tunnel by a 0.1-12 Hz Chirp input to the swashplate. Two different Chirp amplitudes, 3° and 15° were used for UMARC/S. The on-axis response is predicted very well. The off-axis phase angle is more difficult to predict.

This represents the first time a Chirp signal was used to excite the rotor in a tunnel to measure rotor response transfer functions. Chirp provides an alternative way to expediently measure rotor frequencies. Figures 9 and 10 show the transfer function of ζ_{1C}/θ_{1C} and ζ_0/θ_{1C}, where ζ_{1C} and ζ_0 are the cosine and collective components of the blade lead-lag response. From these transfer functions, the cyclic and collective mode frequencies for the 5-bladed S-76 BMR can be identified and used for correlation. In Figs. 9 and 10, $1L_{1r}$, $1L_{1c}$, $1L_{1p}$, $1L_{2r}$, and $1L_{2p}$, are the 1st regressing, collective, 1st progressing, 2nd regressing and 2nd progressing modal frequencies for the first lag mode.

Pushrod Load and Damper Load Predictions

Figure 11 shows the hydraulic damper load predictions for a Black Hawk at 145 kt and 22,000 lb gross weight using RDYNE. The thick solid line is the flight data and the thin solid line is RDYNE prediction utilizing a nonlinear force-velocity damper model. The discontinuous symbols represent RDYNE prediction using a judiciously selected constant damping value. Hydraulic dampers have a very nonlinear force-velocity damping curve, therefore, it is difficult to select an equivalent damping for them. Reference 7 shows that depending on the equivalent damping value selected by the user, the correlation can vary from good to poor. Figure 11 demonstrates that including a nonlinear damper model can offer good prediction without any user interface. When a nonlinear damper model is used, the mounting geometry must be modeled carefully to give the proper relationship between blade motion and damper displacement.

Figure 12 shows the pushrod load prediction for a Sikorsky Black Hawk at 155 kt using four different comprehensive codes: UMARC/S, KTRAN, RDYNE and 2GCHAS. The solid line represents the flight data processed using NASA Ames TRENDS software. RDYNE is the only analysis out of the four that includes a nonlinear hydraulic damper model and modeling for the damper attachment geometry. Therefore, the prediction from RDYNE is slightly better, especially at the retreating side. For Figs. 12-15, Scully wake is used in UMARC/S and 2GCHAS. The Egolf wake is used in RDYNE and KTRAN.

Traditionally, pushrod loads are difficult to predict accurately because they are sensitive to control system stiffness, control input, and blade torsional response. Blade torsional response calculation is a difficult coupled structure-aerodynamic problem. When the calculated torsional response is not accurate, then the angle-of-attack is in error and consequently the airloads are incorrect. When the airloads are incorrect, the torsional response error increases.

Figure 13 shows the pushrod load prediction for the Comanche BMR at 140 kt using UMARC/S. The analysis used a constant stiffness k' and a constant loss factor n for the snubber/damper and yields reasonable results. The loss factor and k' were selected based on the averaged snubber displacement for one rotor revolution as calculated by UMARC/S. Adding a time dependent nonlinear model may improve the prediction for the higher harmonics. A free wake model should always be included in pushrod load predictions [7, 14].

For predicting BMR pushrod loads, it is necessary to have the static calibration information for the

pushrod. The static pushrod load vs. collective curve yields the tare value that needs to be added, and the slope of the line tells us about the combined torsional stiffness of the flexbeam, snubber/damper, and the elastomeric bearing at the pitch link.

Blade Loads Prediction

A prerequisite to accurate hub loads prediction is the ability to accurately predict blade bending moments. Figures 14 and 15 show the flatwise and chordwise bending moments at r/R=0.5 for a Black Hawk at 16,800 lb gross weight and u = .360 (155 kt). Four different analyses were used for the predictions. The spanwise bending moments in harmonic format are shown in Ref. 7 and Fig. 16. The effect of using measured airloads (Cn and Cm) derived from pressure gauges on the instrumented Black Hawk blade is demonstrated in Fig. 16. As expected, using measured airloads instead of calculated airloads, improves the prediction.

Figures 17 and 18 show the predicted root end peak vibratory bending load (at r/R=0.1) for a full-scale VDTR flying in the helicopter mode. For a tiltrotor, the blade loads during the transition mode (80 to 200 kt) are always higher than in the low speed helicopter mode or the high speed airplane mode. Figures 17 and 18 demonstrate that by reducing the rotor diameter, the maximum vibratory load will not grow continuously as airspeed builds up during the conversion mode. The retraction ratios and nacelle tilt angles for the VDTR are shown in the figures.

Figure 19 presents the nondimensionalized flatwise and chordwise bending moments for the S-76 BMR for one rotor revolution, plotted from the flexbeam root (r/R=0.045) to the blade tip. The wind tunnel data were measured at 100 kt tunnel speed and 14,000 lb rotor thrust. The predictions were done with the Sikorsky version of the UMARC with Scully free wake and the KTRAN analysis with Egolf FREEWAKE. Figure 19d shows without a free wake, some of the higher harmonic contents are missing. The 3-dimensional carpet plots are useful in providing a qualitative assessment. Comparing the harmonic content, as shown in Fig. 16, provides a more detailed examination.

Figure 20 shows the nondimensionalized flatwise and chordwise bending moments for the Comanche BMR at 100 kt and 12,500 lb gross weight. The comparisons are shown for the root end of the flexbeam (r/R=0.053) and at r/R=0.36, which is just outboard of the flexbeam, blade and torque tube junction. The discrepancy in the correlation for the chordwise moment at ψ=300° could be due to the high inflow angle on the retreating side. Figure 21 shows the spanwise distribution for the 1-6p harmonics are predicted well. Since the Comanche has a 5-bladed main rotor, the high quality of the predicted 4p and 6p loads at the flexbeam root hints that the fixed frame 5p hub loads will be predicted well.

Hub Loads Prediction

Accurate prediction of vibratory hub loads is one of the most challenging and important tasks in dynamics correlation. The current surge of interest in obtaining a jet-smooth ride has helped place more emphasis on hub loads correlation. Prior to using any aeroelastic code for optimization studies or active control studies, the analysis must be validated first.

Figures 22-24 present the measured and predicted 4p hub loads versus airspeed for a set of baseline experimental blades tested on a Black Hawk. The inplane force in Figure 22 is the vector sum of 4P longitudinal (Fx) and lateral (Fy) forces nondimensionalized by the nominal rotor thrust. The overturning moment in Fig. 24 is defined as the vector sum of the pitching and rolling moments divided by twice the nominal rotor thrust times the dimensional flap hinge offset, e. Black Hawks have a bifilar pendulum absorber mounted on top of the main rotor hub to reduce the 3p inplane hub load in the rotating frame. For the purpose of the correlation, the effect of the bifilar has been removed mathematically. Therefore, the g level shown in Fig. 22 is higher than what is seen in flight.

Only if both the hub loads and fuselage dynamics can be predicted reasonably well, then the cabin vibration can be calculated confidently [21]. Figure 25 shows the NASTRAN modeling for a Sikorsky Black Hawk fuselage. Over 25,000 DOF were included in this finite element model. Figure 26 shows the shake test set up for measuring Black Hawk fuselage mode shapes and frequencies. Shake forces were applied at the rotor hub in one direction at a time. Figure 27 shows the measured and predicted fuselage frequency response function. The quality of the prediction is tabularized in Table 1. The average error for the first ten fuselage modes is less than 3.4%.

Active Control Prediction

The potential use of active control concepts on helicopters is receiving increased attention from both U.S. and European industry. These efforts are being supported by significant amounts of work at universities, material and actuator companies and government research laboratories. Much emphasis has been placed on the requirements for low weight, highly reliable, high authority actuator systems which have been shown to be necessary to yield desired results. The feasibility of any concept selected for active rotor control is directly linked to the capabilities that are emerging in this area. Some of the recent active control work done by Sikorsky Aircraft (from Ref. 22) will be presented here.

The data chosen to validate the Sikorsky UMARC/S active control modules are the IBC results from a full-scale hingeless BO-105 rotor from Ref. 23. The initial focus is on the percentage change in 4P hub loads, relative to a baseline no IBC condition, for phase sweeps at a given amplitude, and amplitude sweeps at a given phase for multiple harmonic IBC inputs.

Figures 28-30 show results for the percent change in 4p inplane shear forces, 4p hub vector moment and 4p lift for a 3p IBC input of 1° amplitude at different phase angles. The flight condition for this point is for an advance ratio of 0.1, Ct/sigma of 0.075 and shaft angle of 2.4° forward. The trends for all three directions are well predicted. Figures 26-28 show for 3p IBC, a phase angle of 150° gives the most reduction in 4p hub loads. The same conclusion is shown by the data and the analysis.

The effects of IBC shake amplitude at a phase angle of 150° are shown in Figs. 31-33. Test data show that a 1° IBC amplitude gives the optimal reduction in 4p vibration. In Figs. 28-33, the moment calculation shows the best correlation with test data.

With a baseline evaluation showing that the UMARC/S analysis gives reasonable representations of vibratory load trends for IBC actuation, results were obtained for additional active control concepts. Figures 34-36 compare predicted results for three different active control concepts: IBC, a 20% span trailing-edge flap (0.7R-0.9R), and internal blade twist actuation. The internal twist actuation (e.g. smart materials embedded in the blade spar) is modeled as a distributed external moment applied uniformly over the entire blade span. An interesting conclusion is that three different active control concepts produce similar vibration control results.

Conclusions

A sample of recent dynamic correlation done at Sikorsky Aircraft has been presented. The current predictive capabilities are better than ever before, however, it is still an on-going challenge to raise the prediction levels higher.

References

1. Ormiston, R. A., Rutkowski, M. J., Ruzicka, G. C., Jung, Y., and Saberi, H., "Comprehensive Aeromechanics Analysis of Complex Rotorcraft using 2GCHAS," Aeromechanics Specialists' Conference, San Francisco, Jan. 1994.

2 Yen, J., Corrigan, J. J., Schillings, J. J., and Hsieh, P. Y., "Comprehensive Analysis Methodology at Bell Helicopter: Copter," Aeromechanics Specialists' Conference, San Francisco, Jan. 1994.

3. Johnson, W., "Technology Drivers in the Development of CAMRAD II," Aeromechanics Specialists' Conference, San Francisco, Jan. 1994.

4. Shultz, L. A., Panda, B., Tarzanin, F. J., Derham, R., Oh, B. K., and Dadone, L., "Interdisciplinary Analysis for Advanced Rotors - Approach, Capabilities and Status," Aeromechanics Specialists' Conference, San Francisco, Jan. 1994.

5. Chopra, I., and Bir, G., "Status of University of Maryland Advanced Rotorcraft Code (UMARC)," Aeromechanics Specialists' Conference, San Francisco, Jan. 1994.

6. Sopher, R., and Hallock, D. W., "Time-History Analysis for Rotorcraft Dynamics Based on a Component Approach," Journal of the American Helicopter Society, Vol. 31, No. 1, Jan. 1986.

7. Wang, J. M., "Challenges of Rotor Dynamics Correlation," American Helicopter Society 54th Annual Forum, Washington, DC, May 1998.

8. Norman, T. R., Cooper, C. R., Fredrickson, C. A., and Herter, J. R., "Full-scale wind Tunnel Evaluation of the Sikorsky Five-bladed Bearingless Main Rotor," American Helicopter Society 49th Annual Forum, St. Louis, MO, May 1993.

9. Wang, J. M., Duh, J., and Fuh, J. S., "Stability of the Sikorsky S-76 Bearingless Main Rotor," American Helicopter Society 49th Annual Forum, St. Louis, MO, May 1993.

10. Wang, J. M., and Norman, T., "Correlation of Flatwise and Chordwise Bending Moments for Sikorsky Bearingless Main Rotor," Aeromechanics Specialists' Conference, San Francisco, Jan. 1994.

11. Wang, J. M., Duh, J., and Fuh, J. S., "Hub Loads Sikorsky S-76 Bearingless Main Rotor," American Helicopter Society 49th Annual Forum, Washington, DC, May, 1994.

12. Kottapalli, S., Swanson, S., LeMasurier, P., and Wang, J. M., "Full-scale Higher Harmonic Control Research to Reduce Hub Loads and," American Helicopter Society 49th Annual Forum, St. Louis, MO, May 1993.

13. Tischler, M. B., Cauffman, M. G., Freedman, C. J., and Driscoll, J. T., "Study of Bearingless Main Rotor Dynamics from Frequency-Response Wind Tunnel Test Data," Aeromechanics Specialists' Conference, San Francisco, Jan. 1994.

14. Wang, J. M., "A Successful Comprehensive Rotor Dynamics Correlation for a Sikorsky Full-scale Bearingless Main Rotor," American Helicopter Society 53rd Annual Forum, Virginia Beach, VA, April 1997.

15. Egolf, T. A., "Helicopter Free Wake Prediction of Complex Wake Structures Under Blade-Vortex Interaction Operating Conditions," American Helicopter Society 44th Annual Forum, Washington DC, June 1988.

16. Wang, J. M., and Chopra, I., "Dynamics of Helicopters with Dissimilar Blades," American Helicopter Society 47th Annual Forum, Phoenix, AZ, May, 1991.

17. Wang, J. M., and Chopra, I., "Dynamics of Helicopters with Dissimilar Blades in Forward Flight,"17th European Rotorcraft Forum, Berlin, Germany, September 1991.

18. Sopher, R., and Chen, S. Y., "Application of Component Mode Synthesis to Modeling the Dynamic Response of Bearingless Main Rotors," American Helicopter Society 48th Annual Forum, Washington, DC, June 1992.

19. Sopher, R., and Duh, J. E., "Prediction of Control System Loads in Level Flight and Maneuvers," American Helicopter Society 50th Annual Forum, Washington, DC, May 1994.

20. Wang, J. M., "Loads and Stability Predictions for a Full-Scale Variable Diameter Tiltrotor," 6th International Workshop on Dynamics and Aeroelastic Modeling of Rotorcraft Systems, Los Angeles, CA, Nov. 1995.

21. Miao, W-L, Twomey, W., and Wang, J. M., "Challenge of Predicting Helicopter Vibration," Helicopter Design Meeting, Gifu, Japan, April 1998.

22. Torok, M. S., "Aeroelastic Analysis of Active Rotor Control Concepts for Vibration Reduction," American Helicopter Society 52nd Annual Forum, Washington, DC, June 1996.

23. Jacklin, S. A., Blaas, A., Teves, D. and Kube, R., "Reduction of Helicopter BVI Noise, Vibration and Power Consumption Through Individual Blade Control," American Helicopter Society 51st Annual Forum, Fort Worth, TX, May 1995.

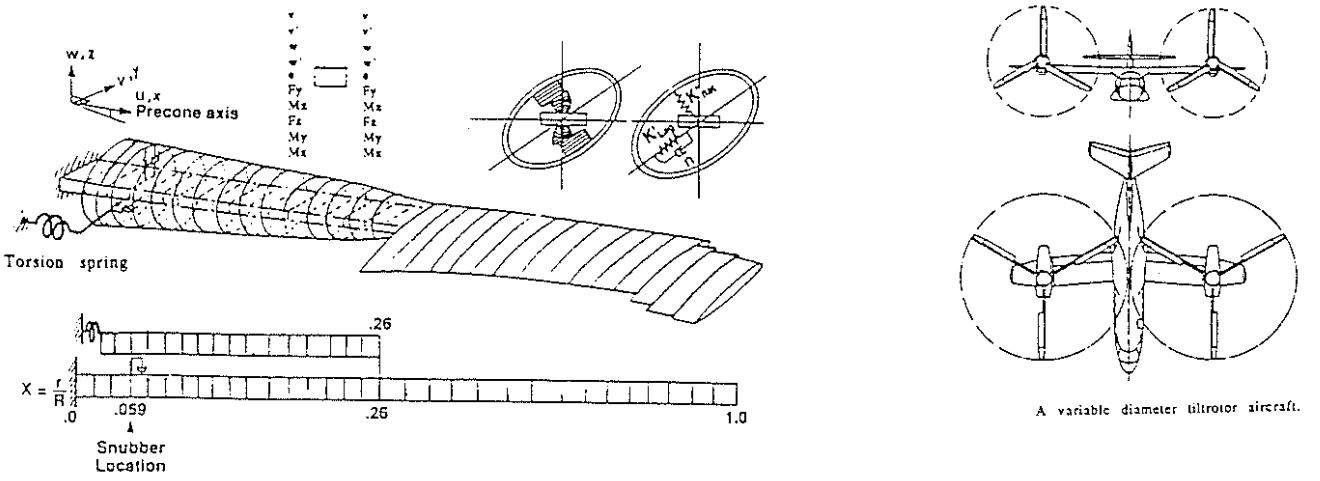

Figure 1. BMR model used by Sikorsky KTRAN analysis.

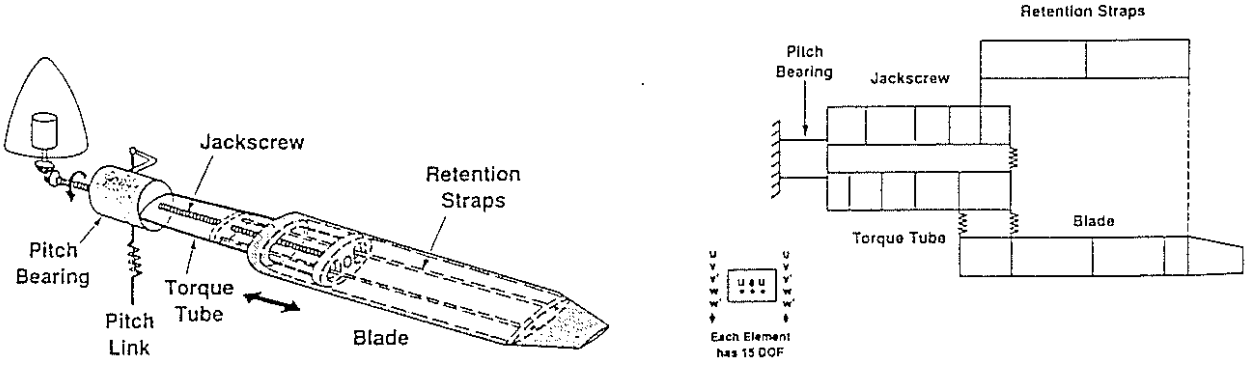

Figure 2. UMARC/S finite element model for the Sikorsky Variable Diameter Tiltrotor (VDTR).

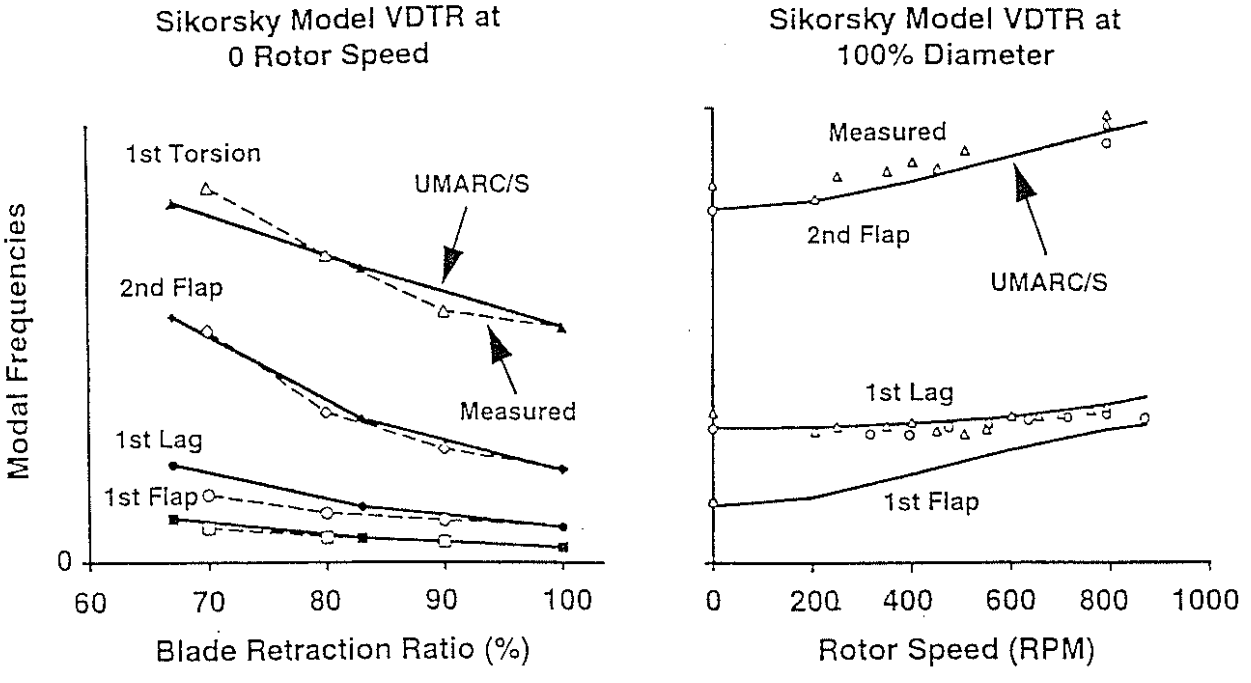

Figure 3. Measured and predicted nonrotating and rotating blade frequencies for VDTR.

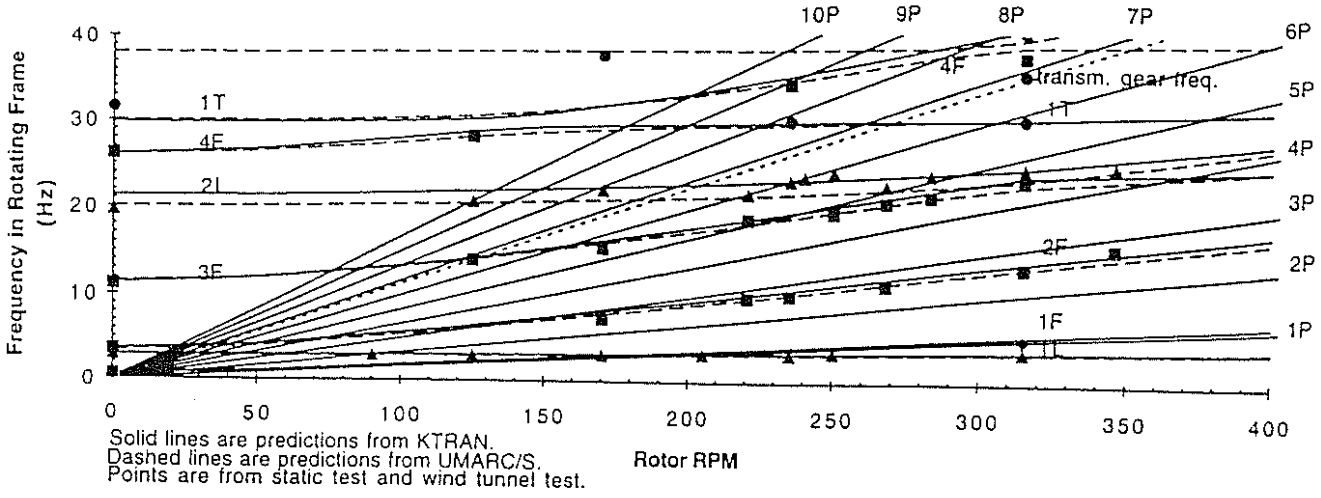

Figure 4. Measured and predicted Southwell plot frequencies for the Sikorsky S-76 BMR.

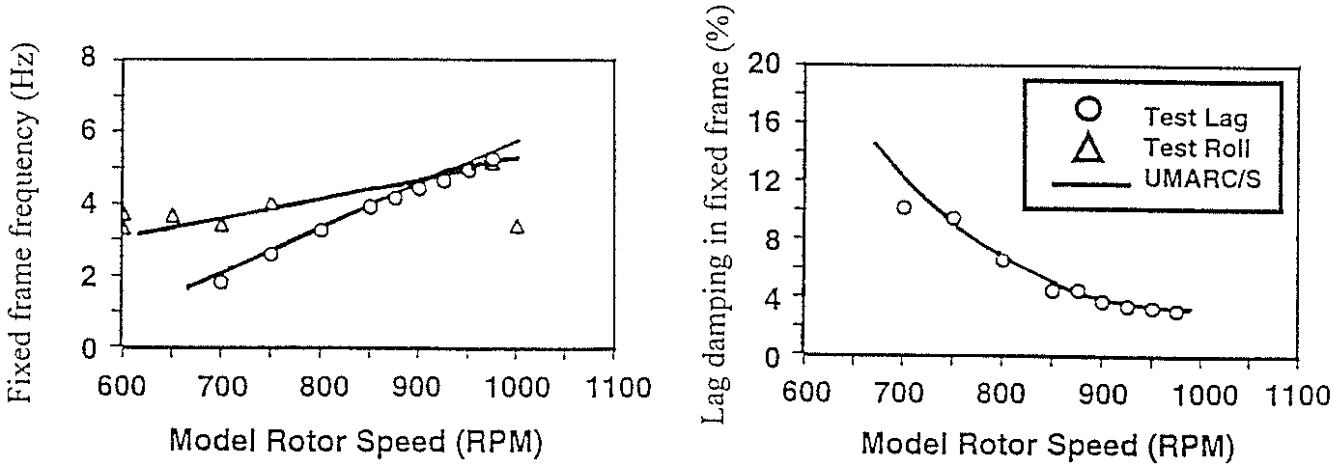

Figure 5. Measured and predicted hover air resonance frequency and damping for the Boeing/Sikorsky model Comanche at 3 degrees collective pitch.

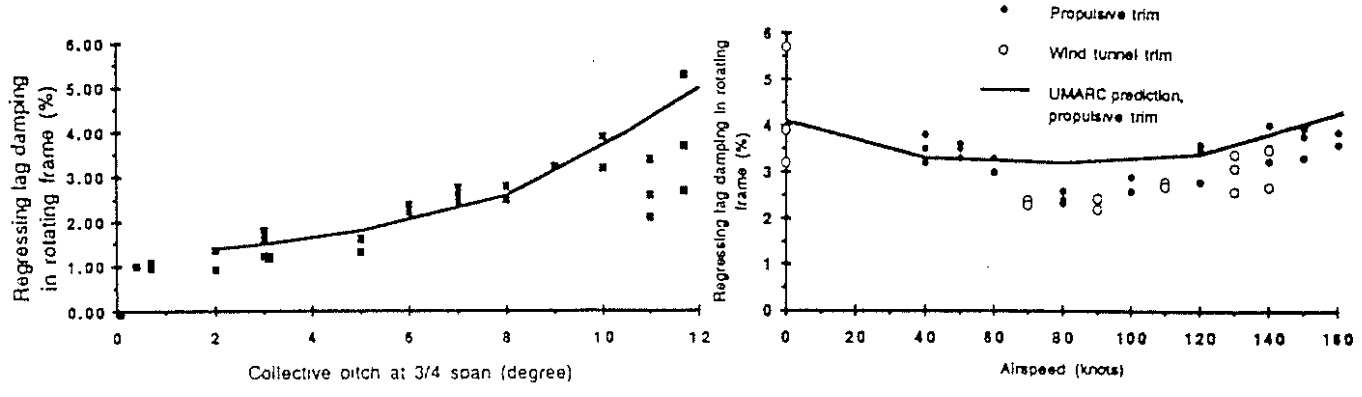

Figure 6. Measured and predicted damping for the Sikorsky 5-bladed S-76 BMR. (Hover condition on the left. Forward flight wind tunnel test conditions on the right, at 14,000 lb thrust.)

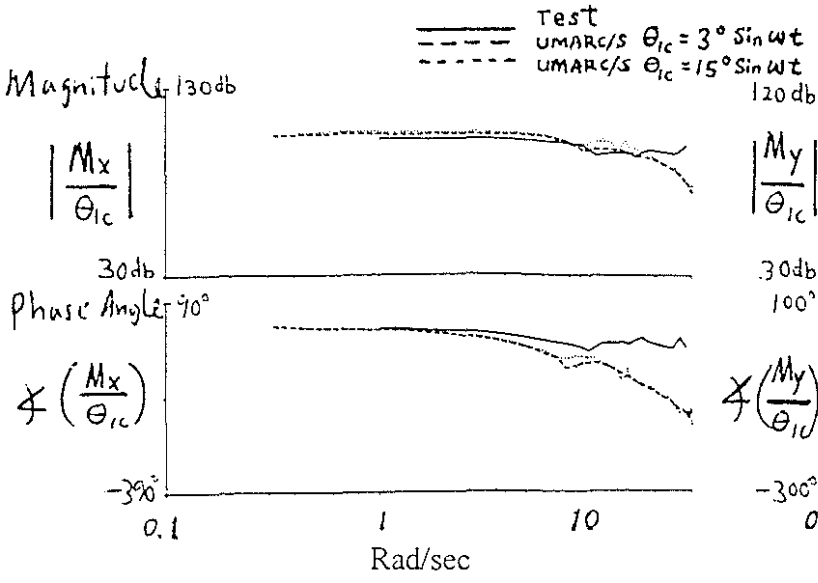

Figure 7. On-axis response transfer function for the S-76 BMR. Mx is the hub rolling moment and θ_{1C} is the lateral cyclic input.

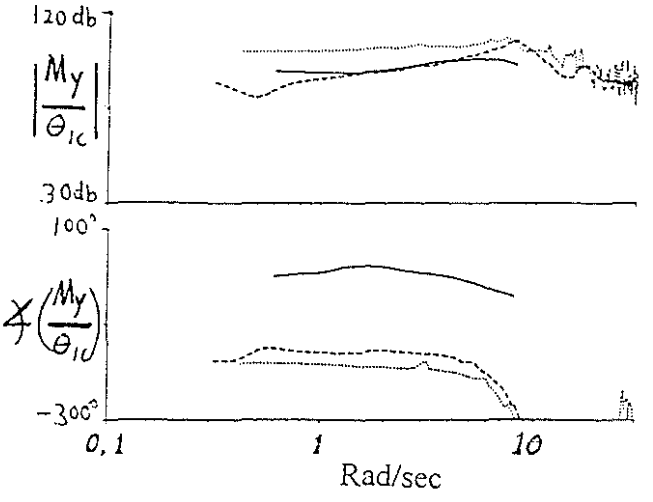

Figure 8. Off-axis response transfer function for the S-76 BMR. My is the hub pitching moment and θ_{1C} is the lateral cyclic input.

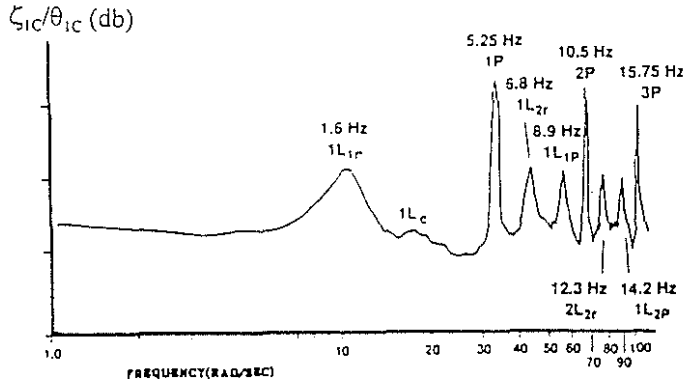

Fig. 9 Bode plot generated from the cosine lag component, $\zeta_{1C}(t)$. A 0.8 to 12 Hz Chirp was used.

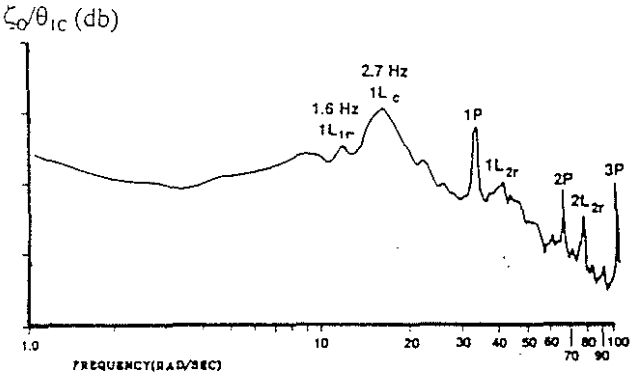

Fig. 10 Bode plot generated from the collective lag component, $\zeta_O(t)$. A 0.8 to 12 Hz Chirp was used.

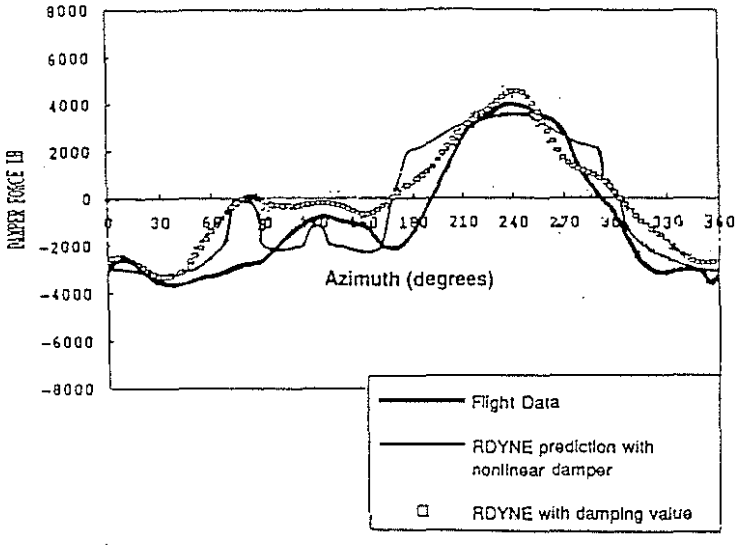

Figure 11. Measured and RDYNE predicted Black Hawk damper load at 145 kt and 22,000 lb gross weight.

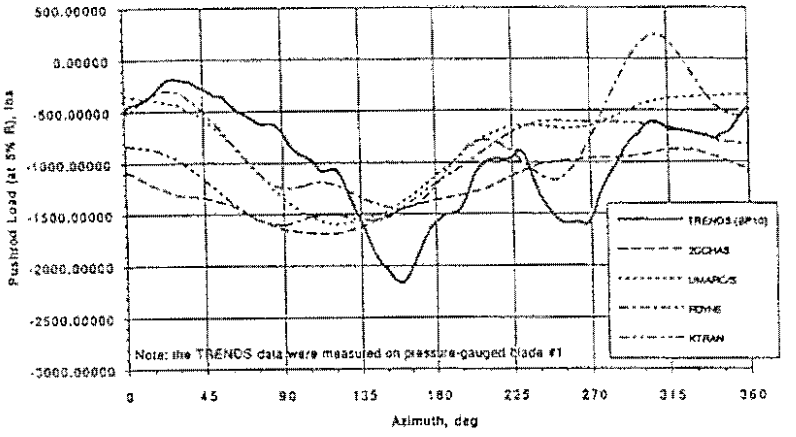

Figure 12. Measured and predicted pushrod load for Black Hawk at 155 kt and 16,800 lb GW. All four analyses include a free wake model.

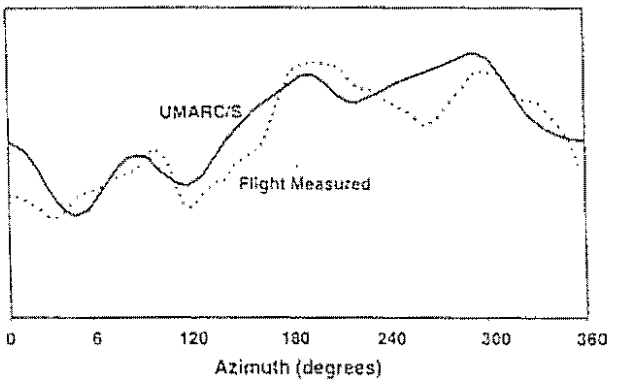

Figure 13. Measured and predicted pushrod load for Comanche at 140 kt.

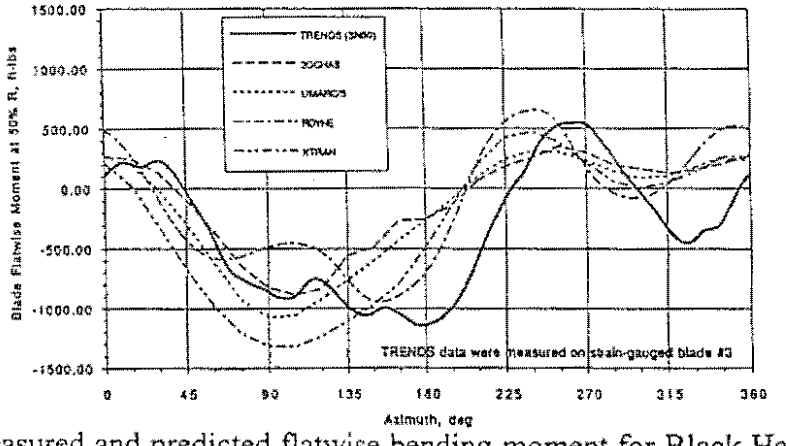

Figure 14. Measured and predicted flatwise bending moment for Black Hawk at 155 kt and 16,800 lb GW. All four analyses include a free wake model.

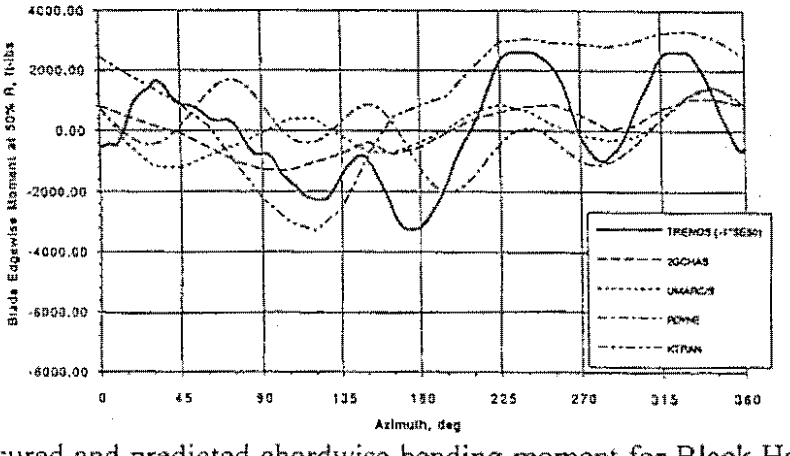

Figure 15. Measured and predicted chordwise bending moment for Black Hawk at 155 kt and 16,800 lb GW. All four analyses include a free wake model.

Figure 16. Measured and predicted flatwise and chordwise bending moment harmonic magnitudes for Black Hawk at 155 kt and 16,800 lb GW.

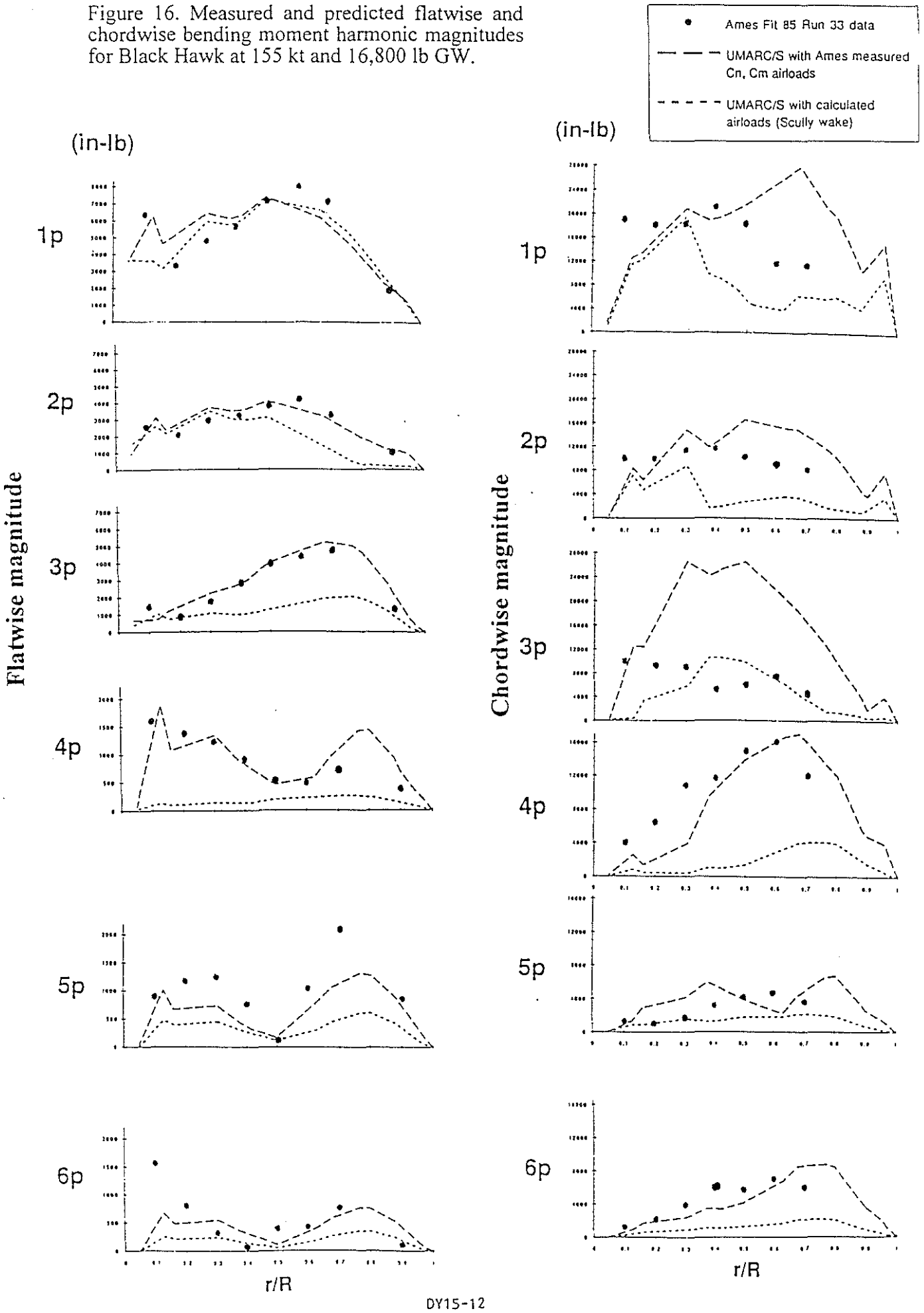

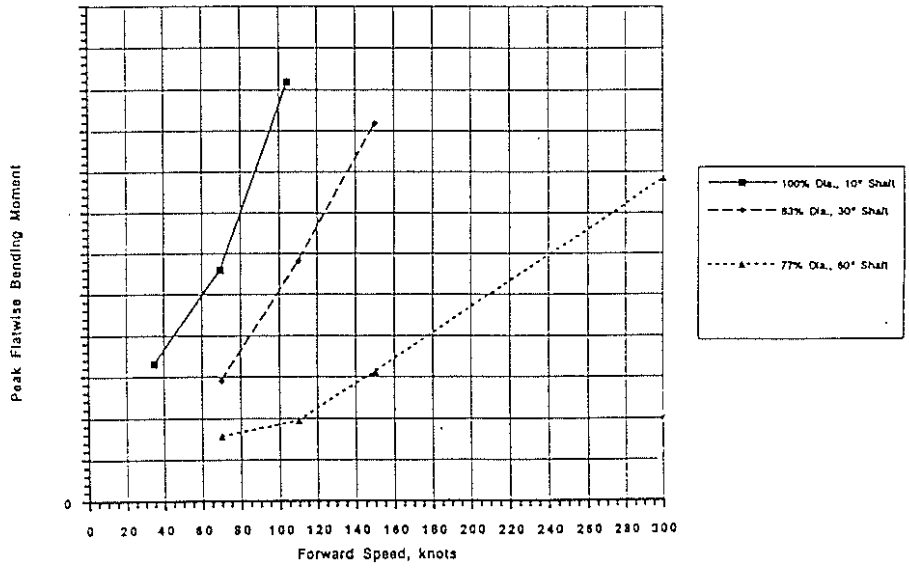

Figure 17. UMARC/S predicted peak flatwise bending moment at r/R=0.1 for a full-scale Variable Diameter Tiltrotor in conversion mode.

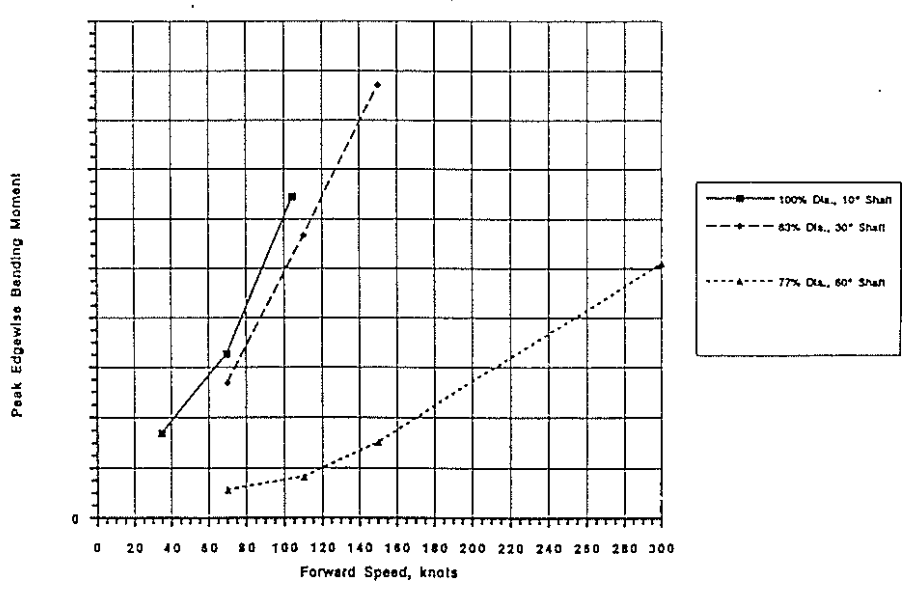

Figure 18. UMARC/S predicted peak chordwise bending moment at r/R=0.1 for a full-scale Variable Diameter Tiltrotor in conversion mode.

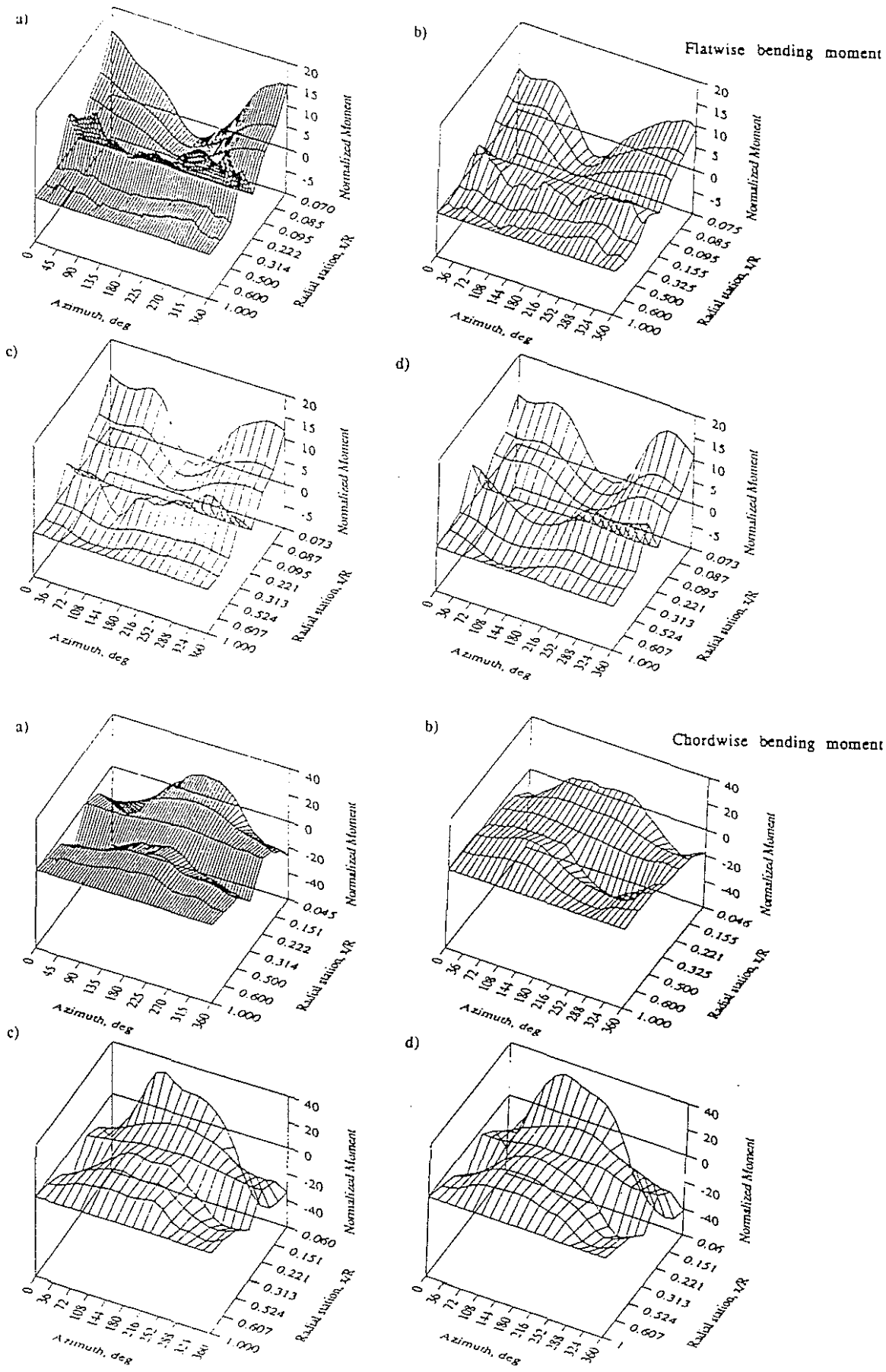

Figure 19. S-76 BMR flatwise and chordwise bending moments at 100 knots, 14000 lb thrust, and 100%Nr, a) measured, b) KTRAN (with Egolf Freewake), c) UMARC/S modal method (with Scully free wake), d) UMARC/S modal method (without free wake).

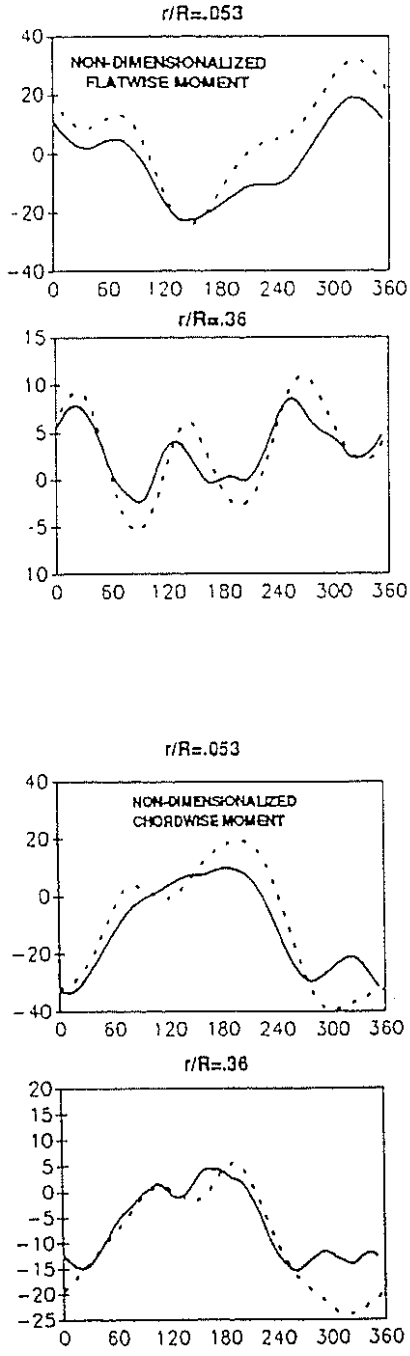

Figure 20. Flight measured and UMARC/S predicted flatwise and chordwise bending moment time histories for the Comanche at 100 kt.

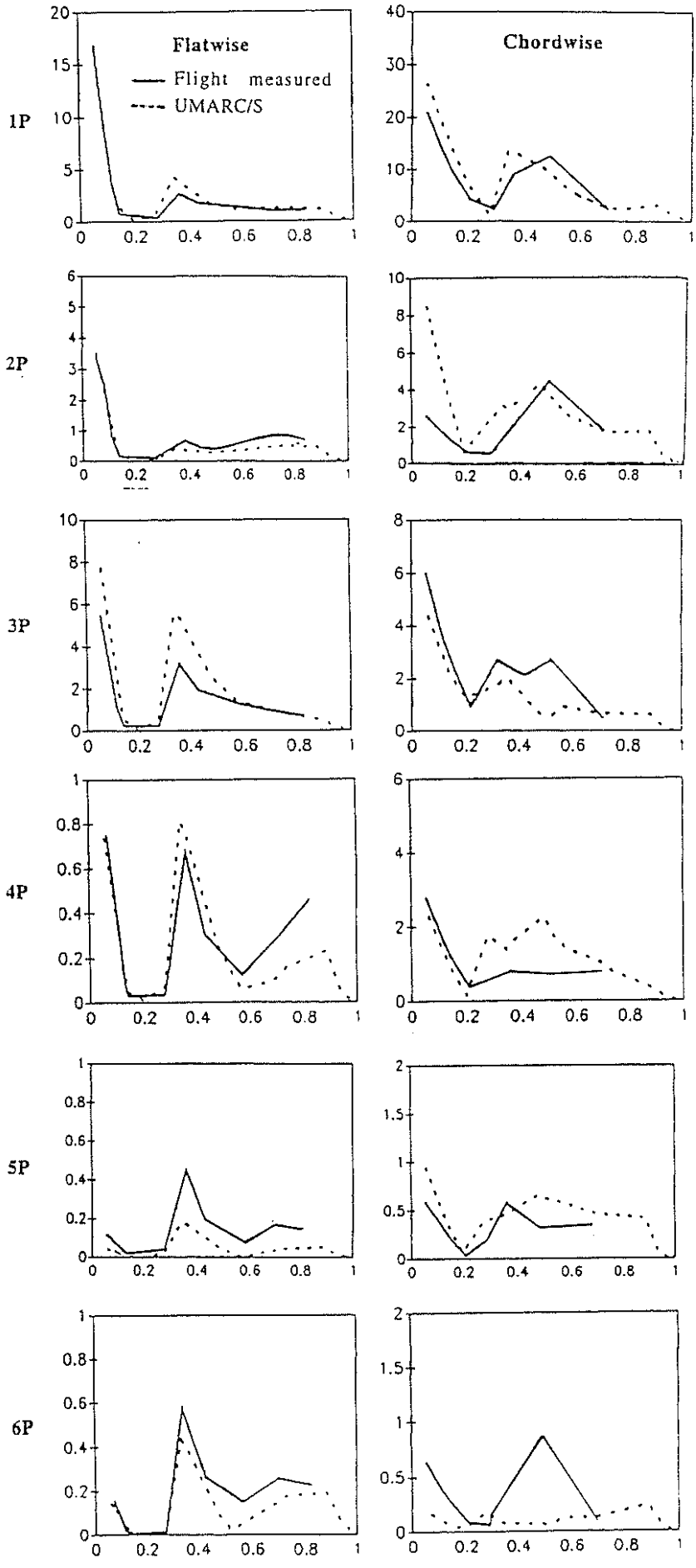

Figure 21. Flight measured and UMARC/S predicted flatwise and chordwise bending moment harmonics for the Comanche at 100 kt.

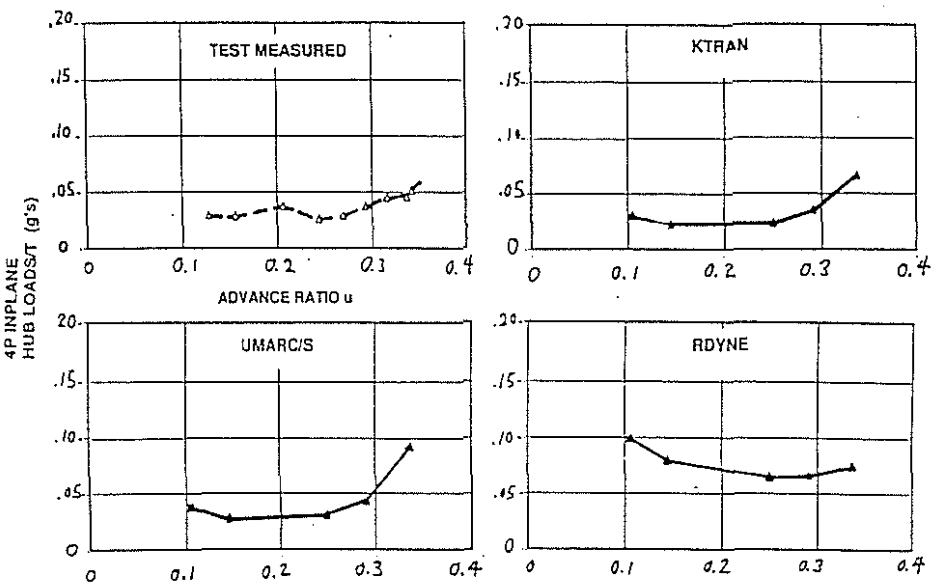

Figure 22. Measured and predicted 4p inplane hub loads for a set of Sikorsky experimental blades tested on a Black hawk.

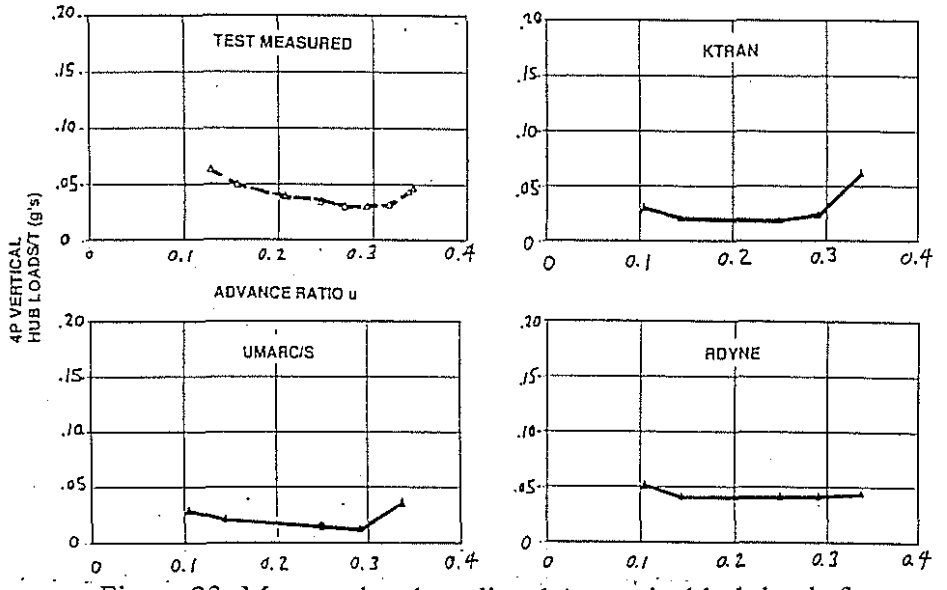

Figure 23. Measured and predicted 4p vertical hub loads for a set of Sikorsky experimental blades tested on a Black hawk.

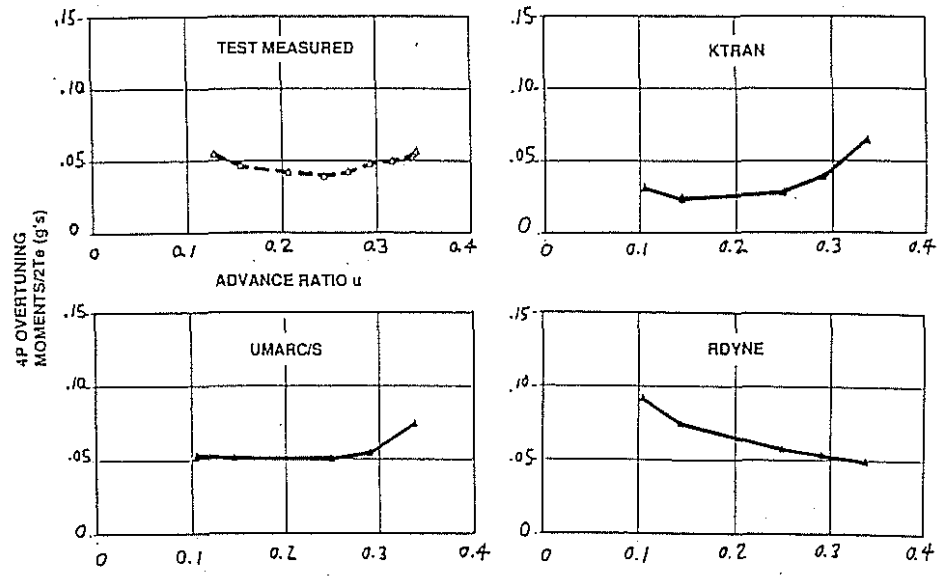

Figure 24. Measured and predicted 4p moment hub loads for a set of Sikorsky experimental blades tested on a Black hawk.

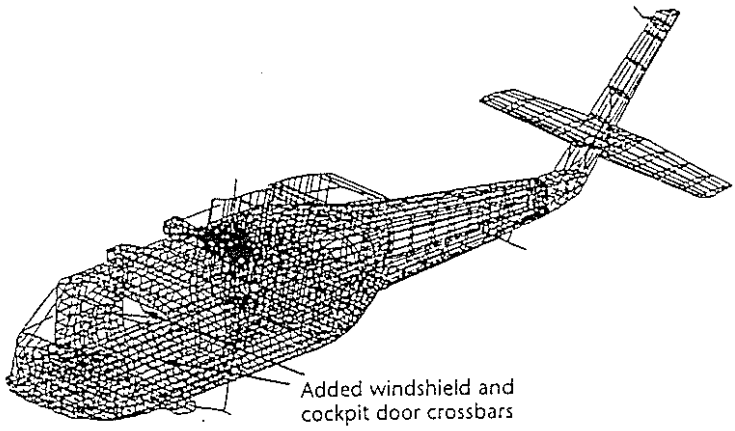

Figure 25. 25,000 DOF NASTRAN FEM model of a Sikorsky Black Hawk.

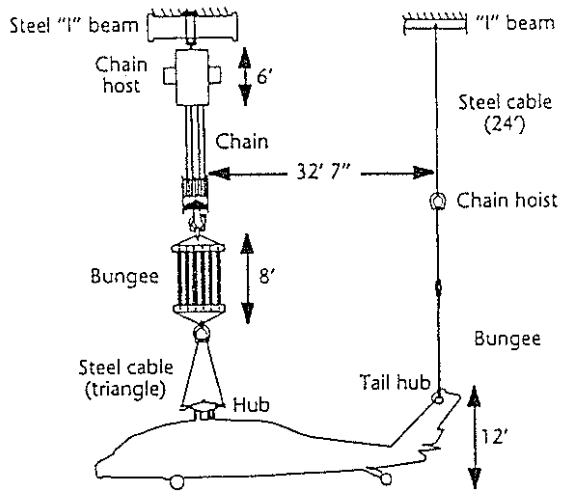

Figure 26. Schematics of the aircraft suspension system during shake test.

Mode	Mode Description	Test Freq. (Hz)	NASTRAN FEM-4 w/Bungee Freq	NASTRAN FEM-4 w/Bungee %Error
1	1st Lateral Bending	5.36	5.02	-6
2	1st Vertical Bending	6.38	6.22	-3
	MR Bungee/Cabin Roll	7.96	7.36	-8
3	Stabilator Roll	9.77	9.68	-1
4	Stabilator Yaw	13. (est)	12.22	-6
5	Xssn Pitch	12.25	12.71	4
6	Xssn Roll/2nd Lat	13.50	13.44	0
7	Same, Opp. Phase	13.94	14.87	7
8	2nd Vertical Bend.	14.10	14.19	1
9	Xssn Vert	15.86	16.89	6
10	Cabin Tors/2nd Lat	17.41	17.53	1
	Average % Error Average MAC			3.4

Table 1. Comparison of measured and NASTRAN predicted fuselage frequencies for a Sikorsky Black Hawk.

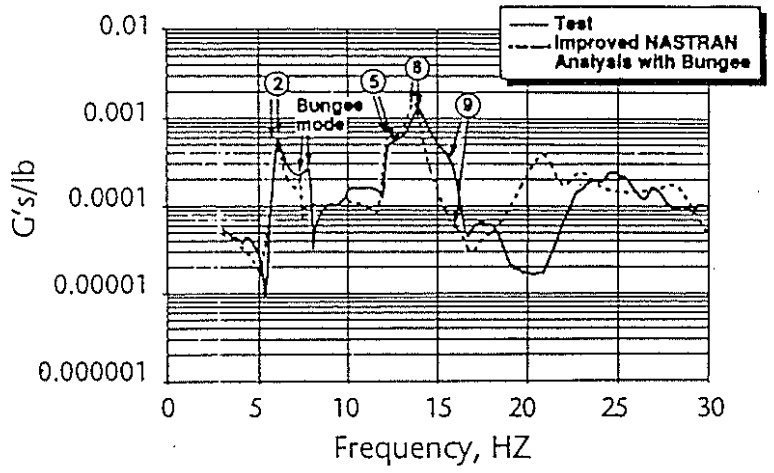

Figure 27. Measured and NASTRAN predicted frequency response function for a Black Hawk fuselage.

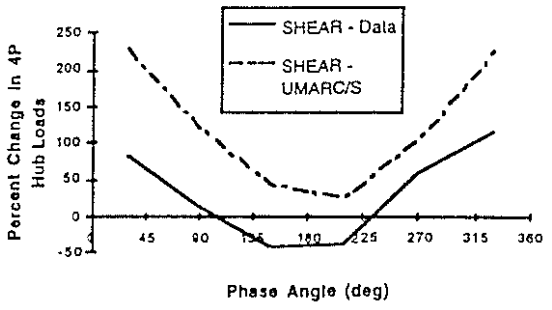

Figure 28. BO-105 IBC SHEAR data vs. UMARC/S, 3P, 1 deg. amplitude input.

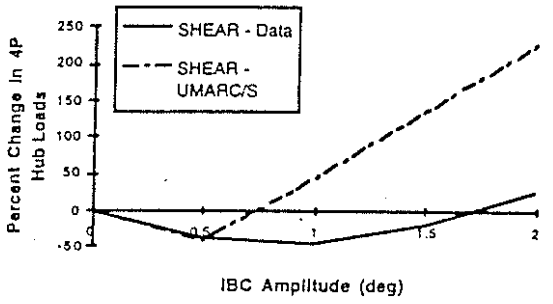

Figure 31. BO-105 IBC SHEAR data vs. UMARC/S, 3P, 150 deg. phase input.

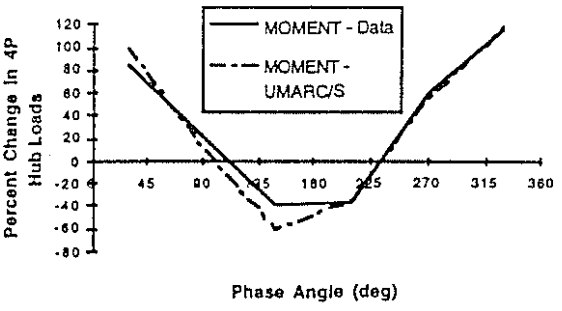

Figure 29. BO-105 IBC MOMENT data vs. UMARC/S, 3P, 1 deg. amplitude input.

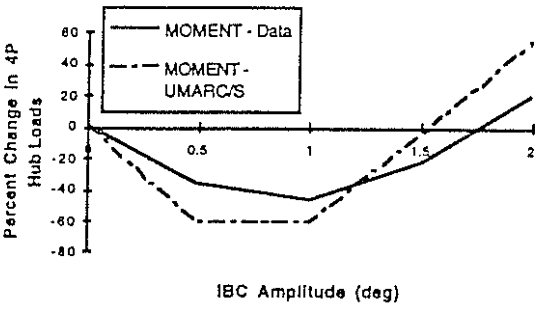

Figure 32. BO-105 IBC MOMENT data vs. UMARC/S, 3P, 150 deg. phase input.

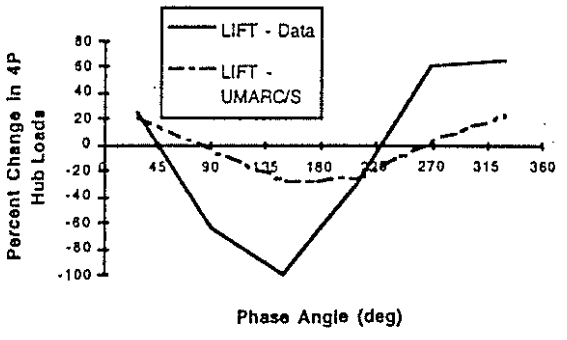

Figure 30. BO-105 IBC LIFT data vs. UMARC/S, 3P, 1 deg. amplitude input.

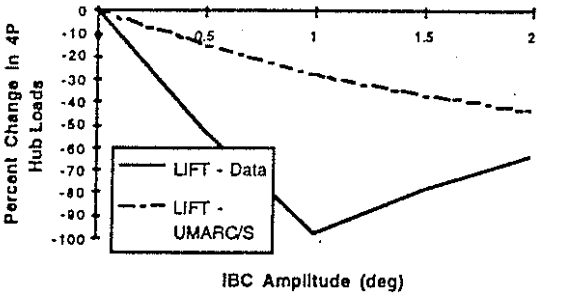

Figure 33. BO-105 IBC LIFT data vs. UMARC/S, 3P, 150 deg. phase input.

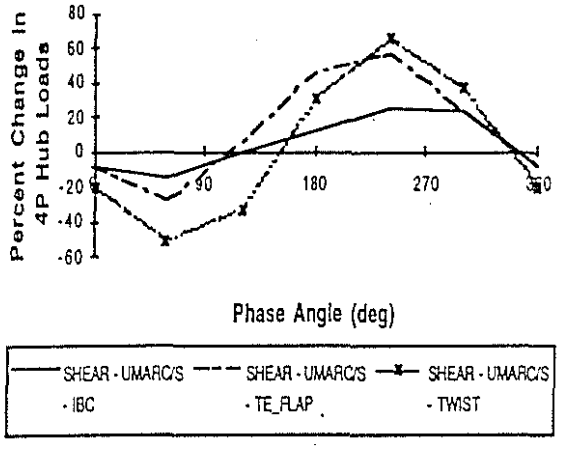

Figure 34. BO-105 SHEAR: IBC vs. Trailing Edge Flap vs. Distributed Twist, UMARC/S, 2P input.

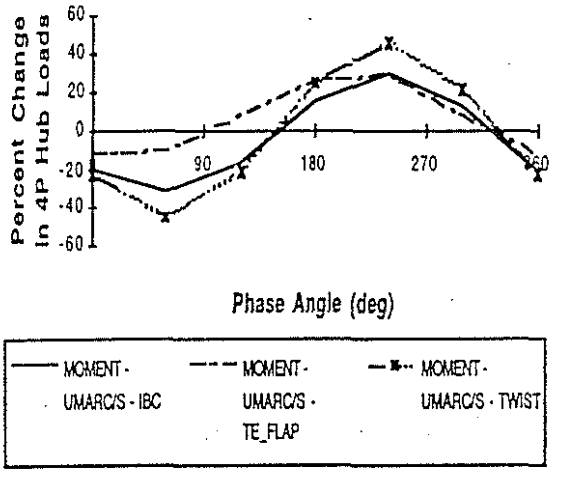

Figure 35. BO-105 MOMENT: IBC vs. Trailing Edge Flap vs. Distributed Twist, UMARC/S, 2P input.

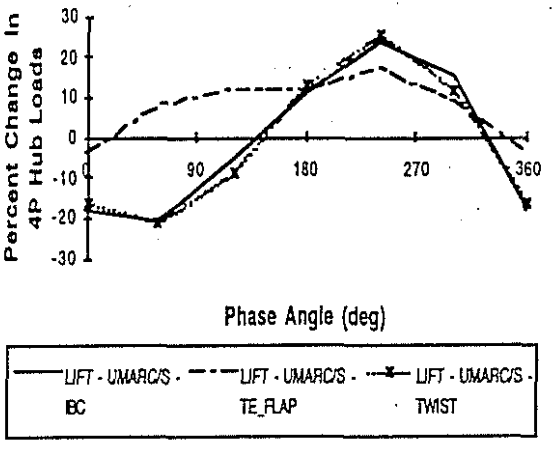

Figure 36. BO-105 LIFT: IBC vs. Trailing Edge Flap vs. Distributed Twist, UMARC/S, 2P input.